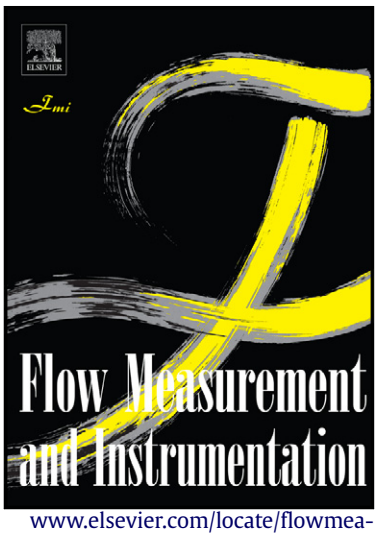

www.elsevier.com/locate/flowmeasinst

Φ-Indices approach and multivariable regression analysis for prediction of discharge in asymmetric straight compound open channel flows

Issam A. Al-Khatib, Mustafa Gogus

PII: S0955-5986(14)00054-5
DOI: http://dx.doi.org/10.1016/j.flowmeasinst.2014.05.010
Reference: JFMI945

To appear in: *Flow Measurement and Instrumentation*

Cite this article as: Issam A. Al-Khatib, Mustafa Gogus, Φ-Indices approach and multivariable regression analysis for prediction of discharge in asymmetric straight compound open channel flows, *Flow Measurement and Instrumentation,* http://dx.doi.org/10.1016/j.flowmeasinst.2014.05.010

Φ-Indices approach and multivariable regression analysis for prediction of discharge in asymmetric straight compound open channel flows

ISSAM A. AL-KHATIB, *Institute of Environmental and Water Studies, Birzeit University, P.O. Box 14, Birzeit, West Bank, Palestine. E-mail: ikhatib@birzeit.edu; ikhatib2012@yahoo.com, Fax: 009722-2982120 (Corresponding Author)*

MUSTAFA GOGUS, *Hydraulics Division, Civil Engineering Department, Middle East Technical University, Ankara, Turkey.*

ABSTRACT: This study is related to flow measurement structures of asymmetric compound cross section mostly suggested for sediment laden- rivers, streams and wadis. Nine different models of asymmetrical rectangular cross sections were tested for a wide range of discharges. In each model, the stages and corresponding discharges were measured. From these measurements, the average discharges utilizing the Φ- Indices Approach were determined. In addition, a multivariable regression model was derived with high accuracy for the prediction of discharge in asymmetric compound channels using five dimensionless parameters.

The measured discharges were compared with the predicted ones obtained from the Φ- indices methods with vertical, horizontal and diagonal interface planes; FI-V, FI-D and FI-H, respectively, with the use of three well-known methods for the computation of the apparent shear stress acting on the interface perimeter, τ_a, and the multivariable regression model for discharge prediction. At lower relative depth values, almost all the tested methods predict discharge with acceptable accuracy. In addition, as the relative depth increases, the results demonstrate a suitable accuracy of the FI-V with the vertical division lines and the multivariable regression model method. The multivariable regression model presented has been identified as the best-fit model in 26 cases out of 29 through minimization of the mean squared errors.

Key Words: Φ- Indices, Compound channel; Division line; Flood plain; Discharge estimation; Regression analysis

1. Introduction

During recent decades, there has been considerable interest in flood channel research parallel to the considerable damage caused by floods and the increased awareness of environmental issues [1, 2]. In the case of rivers with flood-plains, when the depth of the flow exceeds the one of the main-channel, the flood plains carry a part of the total discharge and an interaction happens between the floodplain flow and the main channel flow [3, 4]. An accurate flow prediction in compound channels is required in river engineering for many practical problems [5]. Flood prevention measures such as lowering or smoothing the flood plains and dredging the main channel depends on the hydraulic response that require total discharge computation in compound channels by obtaining stage-discharge relationships [6, 7]. In addition, local flow conditions determine the deposition and erosion rates of sediment in the flood plains and main channel. Therefore, for implying flood mitigation measures, it is essential to predict the discharge capacity of compound channels accurately [3, 8, 9].

Most rivers and wadis flow over their main channel banks during heavy rainfall and invade the surrounding floodplain. When identifying flooded areas from predicted discharges is required, estimating the impact of a mitigation scheme, or flood routing in real time is performed; the modeling of such flows is of primary importance [10-13].

Secondary currents and mixing patterns are generated due to the difference in flow velocity between the flood plain and the main channel when flood plains inundate [14, 15]. Experimental studies indicate that lateral momentum transfer occurs between the flood plains and main channels and generally accelerates the flow into the flood plain

while slowing down the flow into the main channel [16-19]. The whole process resists the flow and lowers the discharge capacity of the compound channel.

In the case of compound open channel flow, the apparent shear stresses are particularly high along the vertical interface at the floodplain - main channel interface [20-23]. While this vertical interface is an appropriate division line to use in vertically divided models, as the Reynolds stresses appear to climax at this location in low overbank flows [21], it is sometimes more appropriate to divide a channel into zones based on zero shear stress lines, as for example in the area and Φ- Indices methods of analysis. This approach is also commonly adopted for the analysis of inbank flows [24-31] but to date less so for analyzing overbank flows.

The aim of this study is to evaluate Φ - indices approach for prediction of discharge in asymmetric straight compound open channel flows through describing the effect of the interaction mechanism on the velocity distribution in asymmetric compound cross sections.

1.1 Theoretical considerations of the Φ- indices methods

This method depends mainly on the force balance in each subsection and takes into consideration the momentum transfer between the main channel and the flood plain. The authors benefited from the procedure presented by Wormleaton and Merrett for the Φ- indices methods [32]. In this method the compound channel is separated from its floodplain by one of the interfaces shown in Fig. 1. Then the forces acting upon each subsection can be defined as follows:

$(Fg)_{mc}$, $(Fg)_f$: The weight components of the fluid in the main channel and floodplain in the direction of flow, respectively.

$(Fb)_{mc}$, $(Fb)_f$: The total boundary shear forces acting on the main channel and floodplain, respectively.

F_a: The apparent shear force acting on the main channel-floodplain interface.

In steady flow conditions these forces must balance within each subsection and therefore for the main channel:

$$(Fg)_{mc} = (Fb)_{mc} + F_a \quad (1)$$

and in terms of shear stress

$$\gamma A_{mc} S_o = \tau_{mc} P_{mc} + \tau_a P_a \quad (2)$$

where τ_{mc} and τ_a are the boundary shear stresses acting on the main channel wetted perimeter, P_{mc}, and the apparent shear stress acting on the interface perimeter, P_a, respectively. A_{mc} is the cross-sectional area of the main channel and γ is the specific weight of water. Eq. (2) is valid for any interface and can be applied to symmetric and asymmetric sections when appropriate values of A_{mc}, P_{mc} and P_a are used. S_o is the bottom slope of the main channel.

From the force balance used in Eq. (2), an expression for the average main channel shear stress can be obtained as:

$$\tau_{mc} = \gamma R_{mc} S_o - \tau_a (P_a / P_{mc}) \quad (3)$$

in which $R_{mc} = A_{mc} / P_{mc}$ = hydraulic radius of the main channel.

The average boundary shear stress, τ_{mc}, can also be expressed in terms of the average main channel velocity, V_{mc}, water density, ρ, and friction coefficient, C_f, as

$$\tau_{mc} = C_f \rho V_{mc}^2 / 2 \quad (4)$$

By combining Eqs. (3) and (4), one can obtain that

$$V_{mc} = \sqrt{\left[\left(2g / C_f\right)\left(R_{mc} S_o - \left(\tau_a P_a / \gamma P_{mc}\right)\right)\right]} \quad (5)$$

where g is the gravity acceleration.

The relationship between the friction coefficient, C_f, and the roughness coefficient of Chezy and Manning is

$$C_f = \frac{2g}{C_h^2} = 2g\left(n^2 / R_{mc}^{1/3}\right) \quad (6)$$

where C_h is the Chézy's resistance factor, and n is the Manning's roughness.

By combining Eqs. (5) and (6), one can show that

$$V_{mc} = V'_{mc}\sqrt{(1 - \tau_a P_a / (\gamma A_{mc} S_o))} \quad (7)$$

where V'_{mc} is the velocity in the main channel given by the Manning formula, if the interface is ignored in assessing the wetted perimeter.

By using Eqs. (2) and (1), Eq. (7) can be written as

$$V_{mc} = V'_{mc}\sqrt{(\tau_{mc} P_{mc} / (\gamma A_{mc} S_o))} = V'_{mc}\sqrt{\left[\left(F_b\right)_{mc} / \left(F_g\right)_{mc}\right]} \quad (8)$$

Wormleaton and Merrett [32] suggested the ratio of boundary shear force to streamwise weight component of the fluid as an index to characterize the degree of interaction between the main channel and floodplain subsection. This index is called as $\varnothing$- index and hence from Eq. (8) it can be written for the main channel as [32]

$$\varnothing_{mc} = \left[\left(F_b\right)_{mc} / \left(F_g\right)_{mc}\right] = \left(V_{mc} / V'_{mc}\right)^2 \quad (9)$$

Therefore Eq (9) can be written in terms of discharge in the main channel, Q_{mc}, if the interface is ignored in assessing the wetted perimeter, Q'_{mc}, and the main channel $\varnothing$ -index, $\varnothing_{mc}$, as

$$Q_{mc} = Q'_{mc} \varnothing_{mc}^{1/2} \quad (10)$$

A similar analysis can be carried out for the floodplain for which the floodplain $\varnothing$ -index, $\varnothing_f$, becomes

$$\varnothing_f = \left[\left(F_b \right)_f / \left(F_g \right)_f \right] \quad (11)$$

Therefore the total discharge for the asymmetric compound channel, Q, becomes

$$Q = Q_{mc} + Q_f = Q'_{mc} \varnothing_{mc}^{1/2} + Q'_f \varnothing_f^{1/2} \quad (12)$$

in which Q_f is the total floodplain discharge, Q'_f is the floodplain discharge if the interface is ignored in assessing the wetted perimeter.

Eq. (12) can be applied to any interface between the main channel and floodplain, providing that the appropriate -Ø indices used.

The use of the Ø- indices to characterize the main channel-floodplain interaction is an advantageous in that they provide an immediate indication of the degree and direction of the momentum transfer across their interface [32]. If the Ø- index is less than unity, then the boundary shear force in the subsection is less than the fluid weight component and so to balance forces, as in Eq. (1), the apparent shear force on the main channel-floodplain interface must act to oppose the flow. Thus, there will be a net flow of momentum out of the subsection across the interface. Conversely, a Ø-index greater than unity will imply that the apparent shear force acts to sustain the flow with consequent net inflow of momentum across the interface. A force balance equation similar to Eq. (2) may be written for the floodplain subsection and ~~it is~~ then by combining it with Eq. (2) to eliminate the apparent shear force term, the following relationship can be obtained.

$$A_f\left(\varnothing_f - 1\right) = A_{mc}\left(1 - \varnothing_{mc}\right) \tag{13}$$

where A_f is the floodplain cross-sectional area. This relationship is valid for any interface.

To be of use in practice, the $\varnothing$- values need to be obtainable from known geometric and roughness properties of the cross section. Only $\varnothing$- values for the main channel need to be calculated in this way, since floodplain values can then be obtained from Eq. (13). For this purpose, from Eqs. (7) and (9), the $\varnothing$-index for the main channel can be put in the form as

$$\varnothing_{mc} = 1 - \left(\tau_a P_a / (\gamma A_{mc} S_o)\right) \tag{14}$$

where

$$P_a = \left(h - z\right) \tag{15}$$

and, here h is the depth of the main channel flow, and z is the height of the main channel step as shown in Fig. 2.

The τ_a formulas published by Baird and Ervine [33], Cristodoulou [34] and Martin-Vide and Moreta [35] (2008) are summarized in Eqs. (16) – (18), respectively, and will be used in the discharge prediction in asymmetric smooth compound channels.

$$\tau_a = \left[\frac{h}{h-z} - 1 + \left(\frac{2z}{B}\right)^{1.25}\right]^{1.5}\left(\frac{2z}{B}\right)^{0.5}\left[0.5 + 0.3ln\left(\frac{B_f}{z}\right)\right].\left(\rho g y_f S_o\right) \tag{16}$$

$$\tau_a = 0.005\rho\left(\frac{B_o}{B}\right)(\Delta V)^2 \quad (17)$$

$$\tau_a = 0.002\rho\frac{B_o}{B}\left(\frac{2z}{B}\right)^{-1/3}\left[\frac{(h-z)}{h}\right]^{-1/3}(\Delta V)^2 \quad (18)$$

where τ_a [N/m^2], ρ [kg/m^3], g [m/s^2], A_{mc} [m^2], S_o [m/m], h [m], z [m], ΔV [m/s], B_f [m], B [m].

The geometric parameters are clarified in Figure 2, where B_f is the width of the floodplain; B = the width of the main channel, B_o = bottom width of the upstream channel, h = main channel water depth; ΔV = the difference in the average velocities in the floodplain and the main channel, as given by the Manning formula. The interface is ignored in the calculation in the wetted perimeter for the purpose of this computation. That is

$$\Delta V = \left|V_{mc}^{'} - V_f^{'}\right| \quad (19)$$

The procedure for the discharge calculation will be analyzed for the three different interface planes, namely:

FI-V: The Ø-indices method with vertical interface plane.

FI-H: The Ø- indices method with horizontal interface plane.

FI-D: The Ø- indices method with diagonal interface plane.

In naming and using short-hand notation; FI stands for Ø-indices; V, H and D stand for vertical, horizontal and diagonal interfaces, respectively. In these methods, the

areas in Eqs. (7), (8), (13) and (14) are computed according to the interface planes chosen.

2. Experimental apparatus and procedure

The authors benefited from the experimental apparatus and procedure presented by Al-Khatib et al. [15] in presenting this section. The experiments were carried out in a glass-walled horizontal laboratory flume 11.0 m long, 0.30 m wide and 0.4 m deep with a bottom slope of 0.0025 at the fluid mechanics laboratory, Mechanical Engineering Department, Birzeit University. Discharge was measured volumetrically with an instantaneous flow meter with 0.1 liter accuracy. A point gauge was used along the centerline of the flume for head measurements. All depth measurements were done with respect to the bottom of the flume.

The models of asymmetric rectangular compound cross sections were fabricated from Plexiglas and placed at about mid length of the laboratory flume. Fig. 2 shows the plan view and cross section of the models with symbols designating important dimensions of the model elements, where θ_1 and θ_2 = entrance angles. The dimensions of the models used in the experiments and all of the related dimensionless parameters are given in Table 1. In this study model types tested are denoted by Mi (i = 1- 9).

The required experiments first were conducted in the models of smallest B (=10 cm) with varying z values (= 4 cm, 6 cm and 8 cm) and then B was increased to 15 cm at the required amount of z (= 4 cm, 6 cm and 8 cm), and finally for B=20 cm with the same three values of z. The entrance angles, θ_1 and θ_2, were 26.565 and 153.35

degrees, respectively. The transition length was twice of the floodplain width, B_f. The discharge values, Q, and the flow depths, h, tested in this study varied between 0.0036 m3/s - 0.0144 m3/s, and 0.065 m and 0.175 m, respectively.

3. Presentation and discussion of results

In the subsequent sections, the variations of the measured (Q_m) and calculated (Q_p) discharges with each other are graphically presented in Figs. 3–20. In each figure, the ranges of B/Z, B_f/B and y_f/Bf ratios in addition to the relative depth, y_f/h, are shown. It is worth mentioning that only two figures out of three figures are presented (by introducing only two values of τ_a from Eqs. (16) – (18) for each model due to the space limitations. In addition to the Φ- Indices methods applied to the 9 tested models, the results of the multivariable regression model represented by Eq. (20) which will be discussed in details in Section 3.4, are also presented in Figs. 3 –20.

3.1. Analysis of the data of model M1 as a sample

Figs. 3 and 4 present the comparison of Φ- Indices methods applied to model M1 by introducing the value of the value of τ_a from Eqs. (16) and (17) respectively with B/Z = 2.5, B_f/B= 2.0, $0.13 \leq y_f/B_f \leq 0.405$, $0.394 \leq y_f/h \leq 0.669$. As shown in Figs. 3 and 4 among the FI methods utilized, FI-V seems to be the best method of discharge calculation for all floodplain depths. Although it overestimates the discharge to a small extent at intermediate floodplain depths, it shows a good fit with the measured discharges for low and high floodplain depths. As the relative depth increases, the momentum transfer and hence the apparent shear stresses decrease over the vertical interface for a given step height. The main reason of this is that at low floodplains there is large apparent shear stress occurring along the vertical interface, but the magnitude of the apparent shear stresses decreases as the floodplain depth increases. Since the apparent shear stresses are neglected in the assumption of FI method; at high floodplain depths the discharge can be predicted much well with the vertical interface. At low relative depths, FI-V, FI-D and FI-H seem to behave in the same way in estimating the discharge as the curves coincide with each other.

3.2. Analysis of the data of other models

From the examination of Figs. 3–20, one can state that almost all of the Φ- Indices methods applied overestimate the discharge for most of the models tested. At lower values of relative depth, y_f/h, most of the calculated discharges coincide with each other and these data approach to the best fit lines of the figures. As the values of y_f/h increase, almost all of Φ- Indices methods overestimate the discharge and FI-V method becomes the best method for discharge estimation, while FI-D and FI-H over estimate the discharge and coincide with each other in most of the nine tested models. It is worth mentioning that the calculated discharges using the three different τ_a formulas (Eqs. 16) - (18)) in the discharge prediction in asymmetric smooth compound channels ~~is~~ are almost the same for each tested model.

3.3. Numerical example

Following is a numerical example for model M4 by introducing the value of τ_a from Eq. (18) with measured discharges for model M4, where B = 0. 15 m, z = 0.04 m, B_f = 0.15 m, $0.167 \leq y_f/B_f \leq 0.473$ and $0.385 \leq y_f/h \leq 0.640$. In Table ~~2~~ in a row, the main channel depth, the measured discharge (Q_m), y_f/B_f and y_f/h are presented in addition to the predicted discharges (Q_p) using the FI-V, FI-D and FI-H methods by utilizing the related equations and the definition of each Φ- Indices method described in Section 1.1. In addition, the predicted discharges determined from Eq. (20) are also presented.

3.4 Multivariable regression analysis

A multivariable regression model has been derived to predict the discharge as a function of y_f, h and the geometry parameters (B, B_f and z) by pooling together the data obtained from the 9 different models of asymmetric compound cross-sections. The derived prediction model is non-linear in form as indicated by Eq. (20) and has been derived as a function of 5 dimensionless parameters, namely, $\frac{y_f}{z}$, $\frac{B_f}{B}$, $\frac{B_f}{z}$, $\frac{B}{z}$, and $\frac{y_f}{h}$ as

$$Ln\left(Q_p\right) = -4.493 + 0.241\left[Ln\left(\frac{y_f}{z}\right)\right]\left[Ln\left(\frac{B_f}{B}\right)\right] - 0.163\left(\frac{B_f}{z}\right)\left[Ln\left(\frac{B_f}{z}\right)\right]$$
$$-0.029\left(\frac{B}{z}\right)^2 + 4.55\left(\frac{Y_f}{h}\right)^{25} + 0.208\left[Ln\left(\frac{y_f}{h}\right)\right]$$

(20)

After performing the necessary linear transformations, the multivariable linear regression techniques have been used to estimate the regression coefficients associated with the derived multivariable regression model. When deriving the empirical model for Q_p as presented in Eq. (20), optimization of 5 main regression statistics was done to reach the best possible prediction equation. The estimated values of the 5 related statistics are given in Table 3.

The corresponding variable coefficient t-statistic values are generally high ranging from -120.100 to 19.157, which results in a confidence level of 99.99%. The Variance Inflation Factor (VIF) is also provided in Table 3. Typically, a VIF value greater than 10 is of concern [36]. The provided values of the VIF indicate that none of them has exceeded the critical VIF value of 10. The empirical prediction model for Q presented in Eq. (20) is significant at a confidence level of 99.99% as the model F-statistic is equal to the value of 1075.330 for Q_p as provided in Table 3. The predictive model has a determination coefficient (R-square) of 0.986. The last statistic used is the model standard error of estimate which is generally small compared to the predicted Q_p values with its value being equal to 0.03974.

The discharge can be predicted with high reliability for a given head h and y_f, ($y_f = h-z$) and the channel cross-section geometry parameters (B, B_f and z) using the multivariable regression model presented in Eq. (20).

3.5 Best-fit prediction model selection

1 As mentioned previously, the predicted discharges (Q_p) using Eq. (20) and the Φ-Indices methods have been plotted in Figs. 3-20 against the corresponding measured discharges (Q_m) for each tested compound channel cross-section type (M1-M9). From these figures, it can be noticed that Eq. (20) almost estimates exactly the discharge of the 9 tested models except the Model M5. However, the best-fit model is identified based on minimizing the mean of squared error (MSE) as defined in Eq. (21) with the error being defined as the difference between the predicted discharge and the corresponding measured value.

$$\mathrm{MSE} = \frac{1}{\mathrm{n}} \sum_{n} \left(Q_p - Q_m \right)^2 \qquad (21)$$

where: Q_p = predicted discharge (m3/s); Q_m = experimentally measured discharge (m^3/s); and n = number of discharge data points used in the analysis.

2 Table 4 provides the best-fit predictive model for each tested compound channel model type (M1–M9). It can be noted that the multi-variable regression model presented in this paper (i.e., Eq. (20)) has been identified as the best-fit model in 26 cases out of 29. Consequently, it can be stated that the presented multivariable regression model is highly reliable in predicting discharge in asymmetric compound rectangular channels.

Conclusions

A series of laboratory experiments have been carried out in an asymmetric straight compound open channel of rectangular cross section with varying main channel and floodplain widths and step height of the main channel. The measured discharges and those obtained from the application of Φ- Indices methods to the nine models tested by introducing the values of τ_a from Eqs. (16) - (18) were presented as a function of B/Z, B_f/B, y_f/B_f, y_f/h. From this study the following conclusions can be drawn:

Almost all of the Φ- Indices methods applied overestimate the discharge for most of the models tested. At lower values of relative depth, y_f/h, mostly all the calculated discharges coincide with each other and approach to the best fit line. As the values of y_f/h increase, FI-V method becomes the best method for discharge estimation, while FI-D and FI-H over estimate the discharge and their data coincide with each other in most of the nine tested models.

A multivariable regression model has been developed through utilizing the experimentally measured discharges as obtained from the nine models. The developed multivariable regression model has been shown to predict the discharge with higher accuracy for the nine tested models than the methods of FI-V, FI-D and FI-H, respectively. The analysis of the empirical formula has highlighted its dependence on the five dimensionless terms including the parameters of the channel cross section and flow depth, namely $\frac{y_f}{z}$, $\frac{B_f}{B}$, $\frac{B_f}{z}$, $\frac{B}{z}$, and $\frac{y_f}{h}$.

~~3~~ The four predicted sets of discharge have been compared to their corresponding experimental values using minimization of the mean of squared errors (MSE). It has been shown that the multivariable regression model presented is the best-fit model in 26 cases out of 29.

Acknowledgements

4 The authors gratefully acknowledge the financial support of the Academic Affairs and the technical support of the Scientific Research Committee at Birzeit University, Palestine.

Notation

The following symbols are used in this paper:

A_f = floodplain cross-sectional area;

A_{mc} = main channel cross-sectional area;

B = width of the main channel;

B_f = bottom width of floodplain;

B_o = bottom width of the upstream channel;

C_f = friction coefficient;

C_h = Chézy's resistance factor;

h = main channel water depth;

Fa = apparent shear force acting on the main channel-floodplain interface;

$(Fb)_f$ = total boundary shear forces acting on the floodplain;

$(Fb)_{mc}$ = total boundary shear forces acting on the main channel;

$(Fg)_f$ = weight components of the fluid in the floodplain in the direction of flow;

$(Fg)_{mc}$ = weight component of the fluid in the main channel in the direction of flow;

FI-D = Ø- indices method with diagonal interface plan;

FI-H = Ø- indices method with horizontal interface plane;

FI-V = Ø-indices method with vertical interface plane;

g = acceleration of gravity;

MSE = mean of squared error

n = Manning's roughness;

P_a = interface perimeter;

P_{mc} = main channel wetted perimeter;

V_{mc} =average main channel velocity;

ρ = water density;

ΔV = the difference in the average velocities in the floodplain and the main channel;

Q = volumetric rate of flow;

Q_{mc} = discharge in the main channel;

Q'_{mc} = discharge in the main channel if the interface is ignored in assessing the wetted perimeter;

$R_{mc} = A_{mc} / P_{mc}$ = hydraulic radius of the main channel;

R-square = determination coefficient;

S_o = bottom slope of the main channel;

VIF = Variance Inflation Factors;

V_{mc} = is the velocity in the main channel;

V'_{mc} = the velocity in the main channel given by the Manning formula, if the interface is ignored in assessing the wetted perimeter;

y_f = floodplain water depth = $h - z$;

z = step height of model cross section;

α = energy correction coefficient;

θ_1 and θ_2 = entrance angles;

$\varnothing_{mc}$ = main channel $\varnothing$ -index;

$\varnothing_f$ = floodplain $\varnothing$ -index;

τ_a = apparent shear stress acting on the interface perimeter;

τ_{mc} = boundary shear stress acting on the main channel wetted perimeter;

γ = specific weight of water.

References

[1] Ozbek T, Kocyigit, MB, Kocyigit O. Comparison of methods for predicting discharge in straight compound channels using the apparent shear stress concept. Turkish J. Eng. Env. Sci. 2004; 28: 101- 109.

[2] Xie Z, Lin B, Falconer RA. Large-eddy simulation of the turbulent structure in compound open-channel flows. Advances in Water Resources 2013; 53: 66-75.

[3] Luo EC. Apparent Shear Stress in Symmetric-Straight Compound-Channel Flow. International Journal of Environmental Protection 2011; 1(2): 28-32.

[4] Peltier Y, Proust S, Riviere N, Paquier A, Shiono K. Turbulent flows in straight compound open-channel with a transverse embankment on the floodplain. J. Hydr. Research 2013; 51(4): 446-458.

[5] Proust S, Fernandes JN, Peltier Y, Leal JB, Riviere N, Cardoso AH. Turbulent non-uniform flows in straight compound open-channels, J. Hydr. Research 2013; 51(6): 1-12.

[6] Kordi E, Ayyoubzadeh SA, Ahmadi MZ, Zahiri A. Prediction of the lateral flow regime and critical depth in compound open channels. Canadian Journal of Civil Engineering 2009; 36: 1–13.

[7] Kordi E, Abustan I. (2011). Estimating the overbank flow discharge using slope-area method. Journal of Hydrologic Engineering, ASCE 2011; 16(11): 907-913.

[8] Huthoff F, Roos PC, Augustijn DCM, Hulscher SJMH. Interacting Divided Channel Method for Compound Channel Flow. Journal of Hydraulic Engineering, ASCE 2008; 134(8): 1158–1165.

[9] Zahiri A, Dehghani AA. Flow discharge determination in straight compound channels using ANNs. World Academy of Science, Engineering and Technology 2009; 34, 12-15.

[10] Bousmar D, Zech Y. Momentum transfer for practical flow computation in compound channels." Journal of Hydraulic Engineering, ASCE 1999; 125(7): 696–706.

[11] Castanedo S, Medina R, Mendez F J. Models for the turbulent diffusion terms of shallow water equations. Journal of Hydraulic Engineering, ASCE 2005; 131(3): 217–223.

[12] Seçkin G. A comparison of one-dimensional methods for estimating discharge capacity of straight compound channels. Can. J. Civ. Eng. 2004; 31(4): 619–631.

[13] Van Prooijen BC, Battjes J A, Uijttewaal WSJ. Momentum exchange in straight uniform compound channel flow. Journal of Hydraulic Engineering, ASCE 2005; 131(3): 175–183.

[14] Yen BC. Open channel flow resistance. Journal of Hydraulic Engineering, ASCE 2002; 128(1): 20–39.

[15] Al-Khatib IA, Dweik AA, Gogus M. Evaluation of separate channel methods for discharge computation in asymmetric compound channels. Flow Measurement and Instrumentation 2012; 24: 19–25.

[16] Atabay S, Knight D W. 1-D modelling of conveyance, boundary shear and sediment transport in overbank flow. Journal of Hydraulic Research 2006; 44(6): 739–754.

[17] Liao H, Knight DW. Analytic stage–discharge formulas for flow in straight prismatic channels. Journal of Hydraulic Engineering, ASCE 2007; 133(10): 1111-1122 .

[18] Jan CD, Chang CF, Kuo FH Experiments on discharge equations of compound broad-crested weirs. J. Irrigation and Drainage Engineering, ASCE 2009; 135(4): 511-515.

[19] Sahu M, Khatua KK, Mahapatra SS. (2011). A neural network approach for prediction of discharge in straight compound open channel flow. Flow Measurement and Instrumentation 2011; 22(5): 438–446.

[20] Knight DW, Demetriou JD. Flood plain and main channel flow interaction. Journal of Hydraulic Engineering, ASCE 1983; 109(8): 1073–1092.

[21] Shiono K, Knight DW. Turbulent open channel flows with variable depth across the channel. Journal of Fluid Mechanics 1991; 222: 617–646.

[22] Ervine DA, Babaeyan-Koopaei K, Sellin RHJ. Two-dimensional solution for straight and meandering overbank flows. Journal of Hydraulic Engineering, ASCE 2000; 126(9): 653–669.

[23] Knight DW, Tang X. Zonal discharges and boundary shear in prismatic channels. Proceedings of the Institution of Civil Engineers Engineering and Computational Mechanics 2008; 161(EM2): 59–68.

[24] Knight DW, Macdonald JA. Open channel flow with varying bed roughness. Journal of the Hydraulics Division, ASCE 1979; 105(HY9): 1167-1183 .

[25] Prinos P, Townsend RD. Comparison of Methods for Predicting Discharge in Compound Open Channels. Adv. In Water Resources 1984; 7: 180-187.

[26] Guo J, Julien PY. Shear stress in smooth rectangular open-channel flows. Journal of Hydraulic Engineering, ASCE 2005; 131(1): 30–37.

[27] Yang SQ, Lim SY. Mechanism of energy transportation and turbulent flow in a 3D channel. Journal of Hydraulic Engineering, ASCE 1997; 123(8): 684–692.

[28] Khodashenas SR, Paquier A. A geometrical method for computing the distribution of boundary shear stress across irregular straight open channels. Journal of Hydraulic Research, 1999; 37(3): 381–388.

[29] Yang SQ, Lim SY. Boundary shear stress distributions in trapezoidal channels. Journal of Hydraulic Research 2005; 43(1): 98–102.

[30] Yang SQ, Lim SY, Mccorquodale JA. Investigation of near wall velocity in 3-D smooth channel flows. Journal of Hydraulic Research 2005; 43(2): 149–157.

[31] Bilgil A. Correlation and distribution of shear stress for turbulent flow in a smooth rectangular open channel. Journal of Hydraulic Research 2005; 43(2): 165–173.

[32]Wormleaton PR, Merrett DJ. An improved method of calculation for steady uniform flow in prismatic main channel/flood plain sections. Journal of Hydraulic Research 1990; 28(2): 157-174

[33] Baird JI, Ervine DL. Resistance to flow in channels with overbank floodplain flow" *Proc. 1st Int. Conf. Channels and Channel Control Structures,* Southampton, U.K. 1984; 4/137- 4/150.

[34] Cristodoulou GC. Apparent shear stress in smooth compound channels. Water Resources Management 1992; 6(3): 235-247.

[35] Martin-Vide JP, Moreta PJM. Formulae for apparent shear stress in straight compound channels with smooth floodplains, in River Flow 2008: Proceedings of the International Conference on Fluvial Hydraulics Cesme-Izmir, Turkey, 3 –5 September 2008; edited by M. S. Altinakar et al., pp. 465– 476, Congr. Dep. and Travel Serv., Ankara.

[36] Kutner MH, Nachtsheim CJ, Neter J. Applied Linear Regression Models, 4th edition 2004; McGraw-Hill Irwin.

Table 1. Dimensions of the recommended models

Types of models	B (cm)	z (cm)	B_f (cm)	B_o (cm)	θ_1 (degrees)	θ_2 (degrees)	B/z (-)	B_o/B (-)	B_f/B (-)	B_o/B_f (-)
M1	10	4	20	30	26.57	153.43	2.50	7.50	2.0	1.5
M2	10	6	20	30	26.57	153.43	1.67	5.00	2.0	1.5
M3	10	8	20	30	26.57	153.43	1.25	3.75	2.0	1.5
M4	15	4	15	30	26.57	153.43	3.75	7.50	1.0	2.0
M5	15	6	15	30	26.57	153.43	2.50	5.00	1.0	2.0
M6	15	8	15	30	26.57	153.43	1.88	3.75	1.0	2.0
M7	20	4	10	30	26.57	153.43	5.00	7.50	0.5	3.0
M8	20	6	10	30	26.57	153.43	3.33	5.00	0.5	3.0
M9	20	8	10	30	26.57	153.43	2.50	3.75	0.5	3.0

Table 2. Numerical example for M4 model.

h	Q_m	y_f/B_f	y_f/h	Q_p (m^3/sec)			
(m)	(m^3/sec)	(-)	(-)	F-IV	FI-D	FI-H	Eq. (20)
0.111	0.0144	0.473	0.640	0.0147	0.0148	0.0165	0.0134
0.109	0.0133	0.460	0.633	0.0143	0.0143	0.0160	0.0129
0.108	0.0128	0.453	0.630	0.0140	0.0133	0.0157	0.0126
0.104	0.0117	0.427	0.615	0.0131	0.0121	0.0146	0.0116
0.103	0.0108	0.420	0.612	0.0129	0.0109	0.0143	0.0113
0.100	0.0100	0.400	0.600	0.0122	0.0107	0.0135	0.0106
0.095	0.0092	0.367	0.579	0.0112	0.0098	0.0122	0.0094
0.089	0.0081	0.327	0.551	0.0099	0.0090	0.0107	0.0082
0.084	0.0069	0.293	0.524	0.0089	0.0076	0.0095	0.0072
0.079	0.0061	0.260	0.494	0.0079	0.0061	0.0083	0.0062
0.074	0.0050	0.227	0.459	0.0070	0.0056	0.0071	0.0054
0.065	0.0039	0.167	0.385	0.0054	0.0046	0.0053	0.0041

Table 3. Summary of statistics multiple regression predictive models

Predictive Model	Model R-Square	Model Standard Error	Model F-Statistic	Model Coefficients	Coefficient t-Statistic	Coefficient VIF	Confidence Level
Ln Q_p	0.986	0.03974	1075.330	-	-	-	-
				-4.493	-120.100	-	99.9%
				0.241	19.157	1.019	99.9%
				-0.163	-53.488	2.687	99.9%
				-0.029	-34.231	1.870	99.9%
				4.550	38.426	7.786	99.9%
				0.208	7.819	5.014	99.9%

Table 4. The best discharge computation methods for the models tested

Model type	τ_a Eq. No.	Range of Y_f/Y_{mc}	Range of Y_f/B_f	The best prediction method
M1	(16)	0.394- 0.669	0.130 - -0.405	Eq. (20)
	(17)	0.394 –0.669	0.130- 0.405	Eq. (20)
	(18)	0.394 -0.669	0.130- 0.405	Eq. (20)
M2	(16)	0.268 – 0.559	0.110 – 0.380	Eq. (20)
	(17)	0.268 – 0.559	0.110 – 0.380	Eq. (20)
	(18)	0.268 – 0.559	0.110 – 0.380	Eq. (20)
M3	(16)	0.158 – 0.543	0.075 – 0.475	FI-D
	(17)	0.158 – 0.543	0.075 – 0.475	Eq. (20)
	(18)	0.158 – 0,543	0.075 - 0.475	Eq. (20)
M4	(16)	0.385 – 0.64	0.167 – 0.473	Eq. (20)
	(17)	0.385 – 0.64	0.167 – 0.473	Eq. (20)
	(18)	0.385 – 0.64	0.167 – 0.473	Eq. (20)
M5	(16)	0.155 - 0.504	0.073-0.407	FI-V
	(17)	0.155 – 0.504	0.073- 0.407	Eq. (20)
	(18)	0.155 – 0.504	0.073- 0.407	FI-D
M6	(16)	0.111– 0.506	0.067 – 0.547	Eq. (20)
	(17)	0.111- 0.506	0.067 – 0.547	Eq. (20)
	(18)	0.111- 0.506	0.067 – 0.547	Eq. (20)
M7	(16)	0.268 – 0.649	0.16 – 0.74	Eq. (20)
	(17)	0.268 – 0.649	0.16 – 0.74	Eq. (20)
	(18)	0.268 – 0.649	0.16 – 0.74	Eq. (20)
M8	(16)	0.167 – 0.512	0.12 - 0.63	Eq. (20)
	(17)	0.167 – 0.512	0.12 - 0.63	Eq. (20)
	(18)	0.167 – 0.512	0.12 - 0.63	Eq. (20)
M9	(16)	0.158 – 0.47	0.15 – 0.71	Eq. (20)
	(17)	0.158 0.47	0.15 – 0.71	Eq. (20)
	(18)	0.158 – 0.47	0.15 – 0.71	Eq. (20)

Highlights

- Φ-Indices approach for prediction of discharge in compound channels was investigated
- Regression analysis was used in the prediction of discharge
- Suitable and the best discharge computation methods were investigated

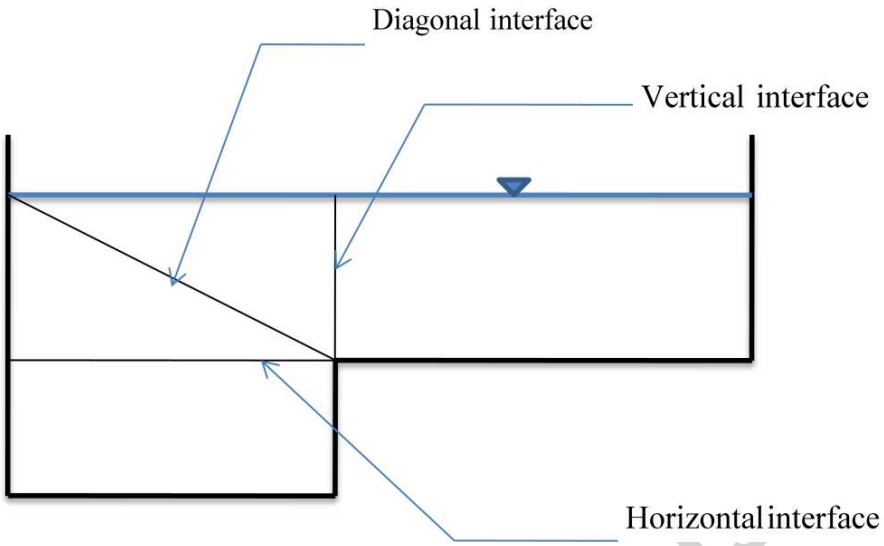

Fig. 1. Channel subdivision lines for asymmetric compound channels

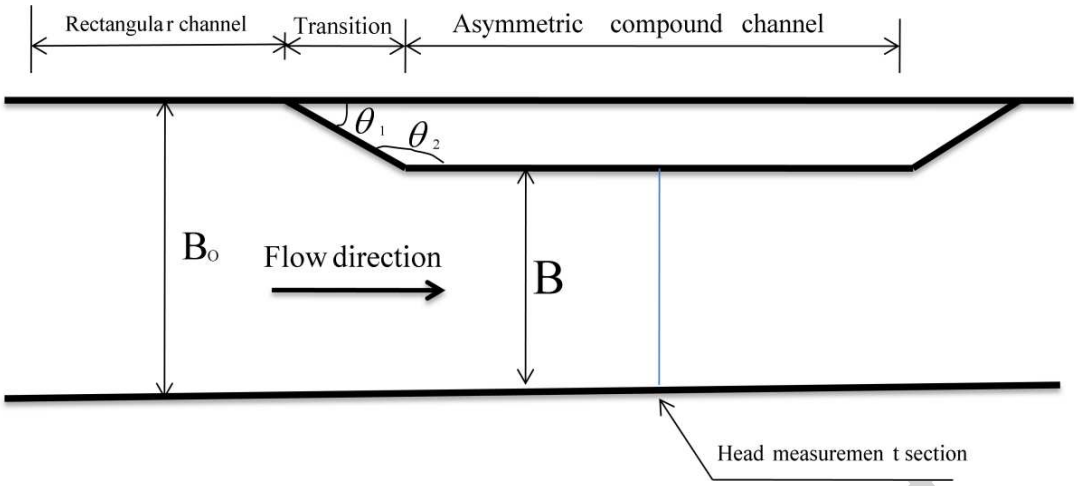

a) Plan view

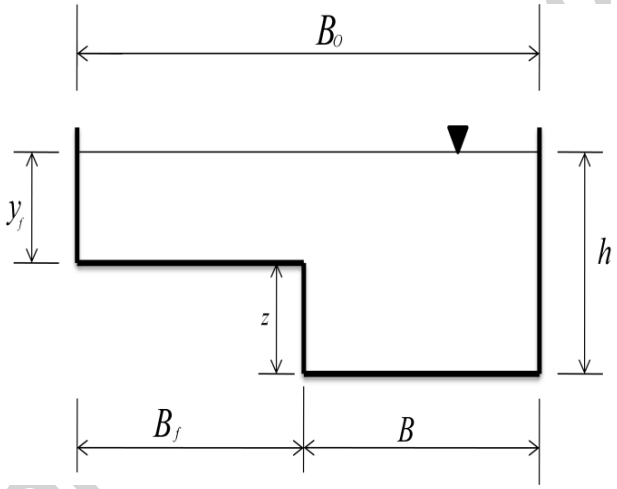

b) Typical cross-section of the asymmetric rectangular compound channel

Fig. 2. Definition sketch of the flume used in the experiments

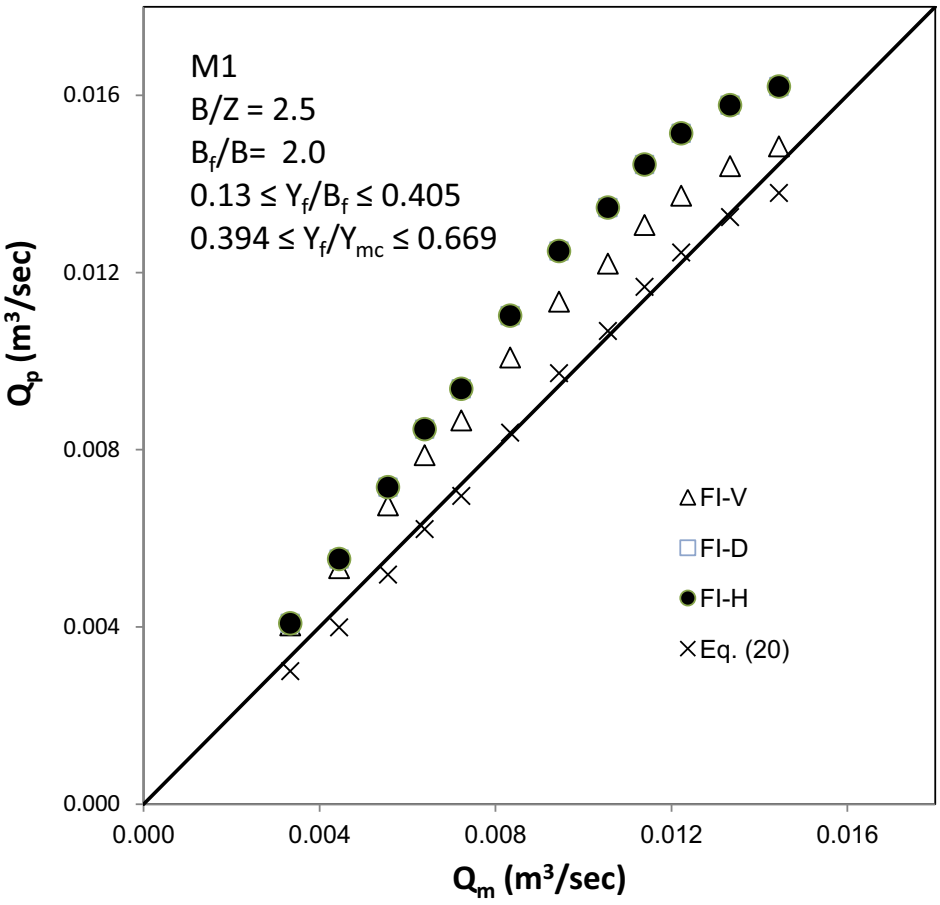

Fig. 3. Comparison of discharge calculation methods by introducing the value of τ_a from Eq. (16) with measured discharges for model M1

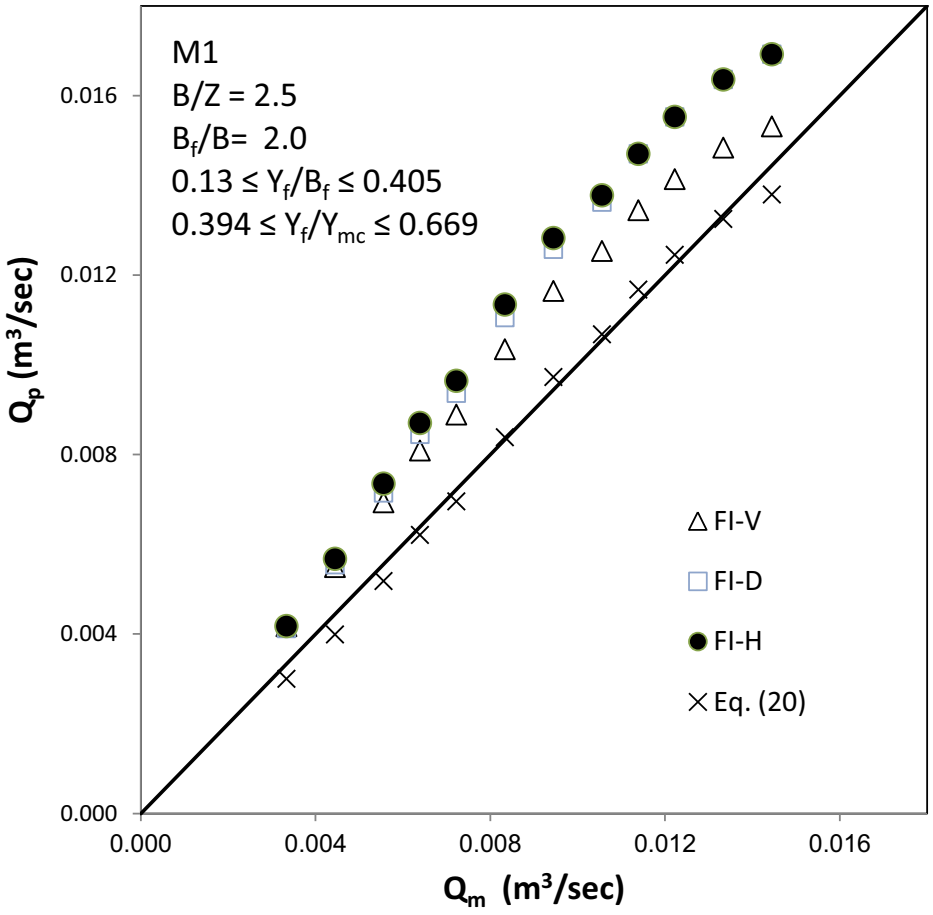

Fig. 4. Comparison of discharge calculation methods by introducing the value of τ_a from Eq. (17) with measured discharges for model M1

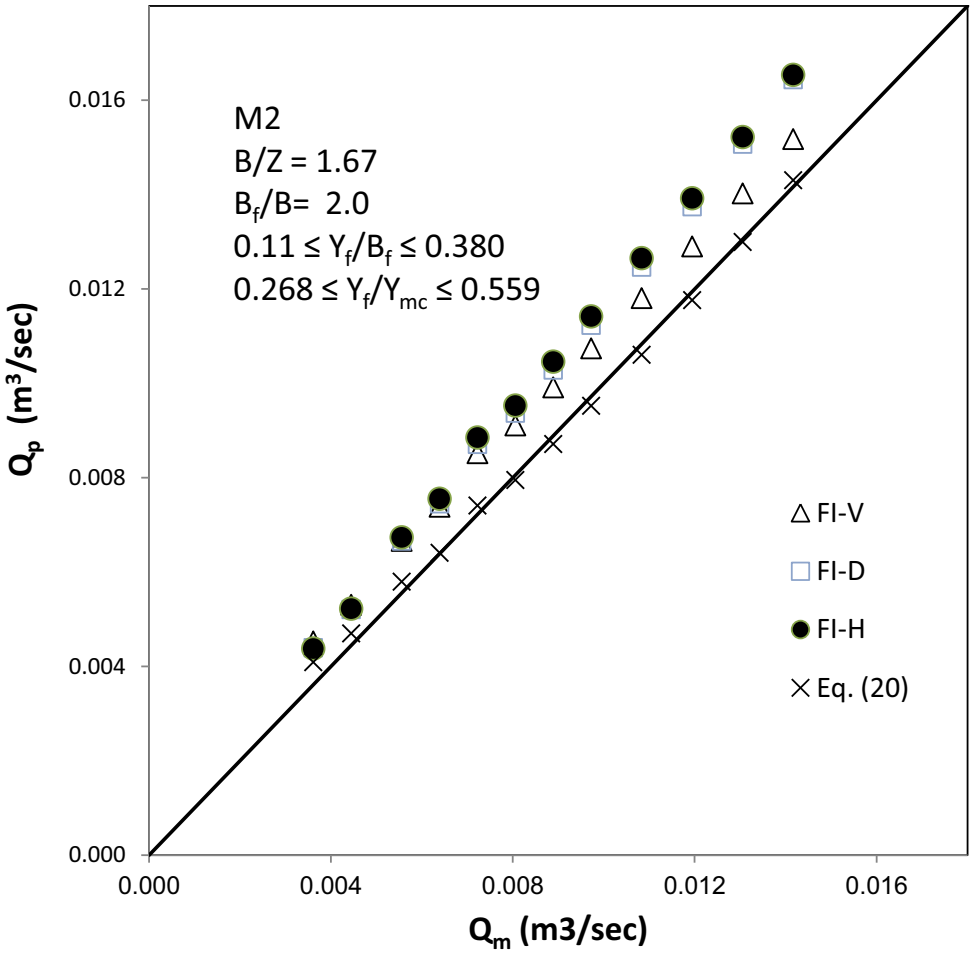

Fig. 5. Comparison of discharge calculation methods by introducing the value of τ_a from Eq. (17) with measured discharges for model M2

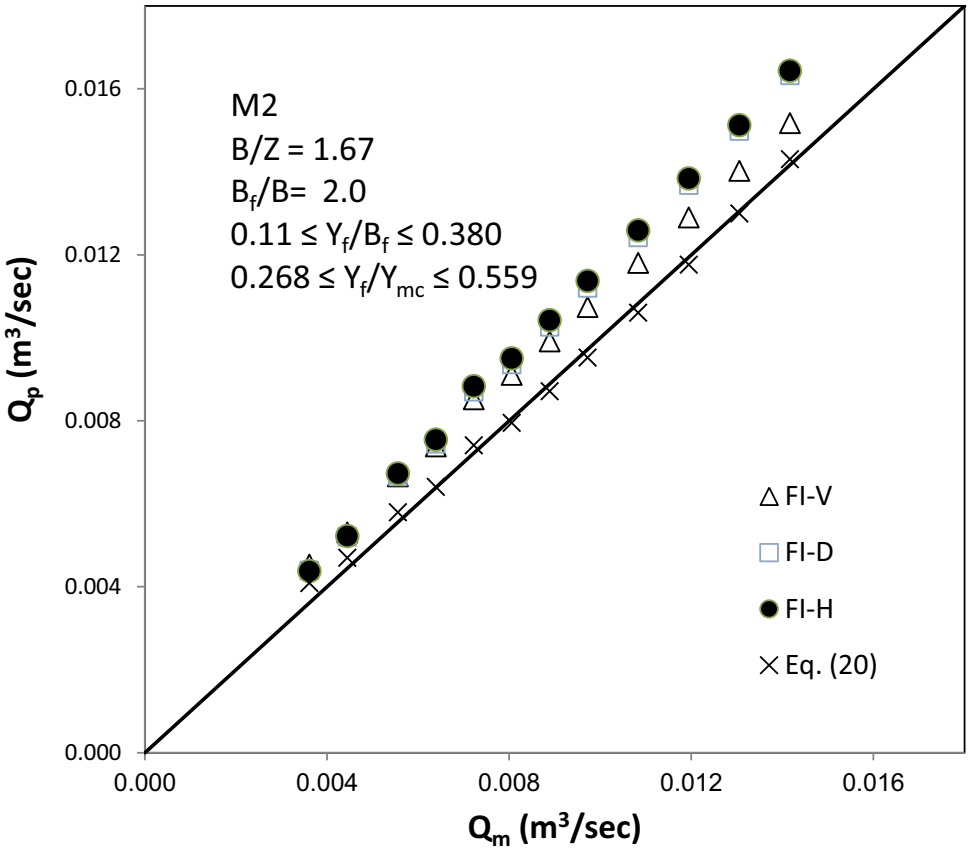

Fig. 6. Comparison of discharge calculation methods by introducing the value of τ_a from Eq. (18) with measured discharges for model M2

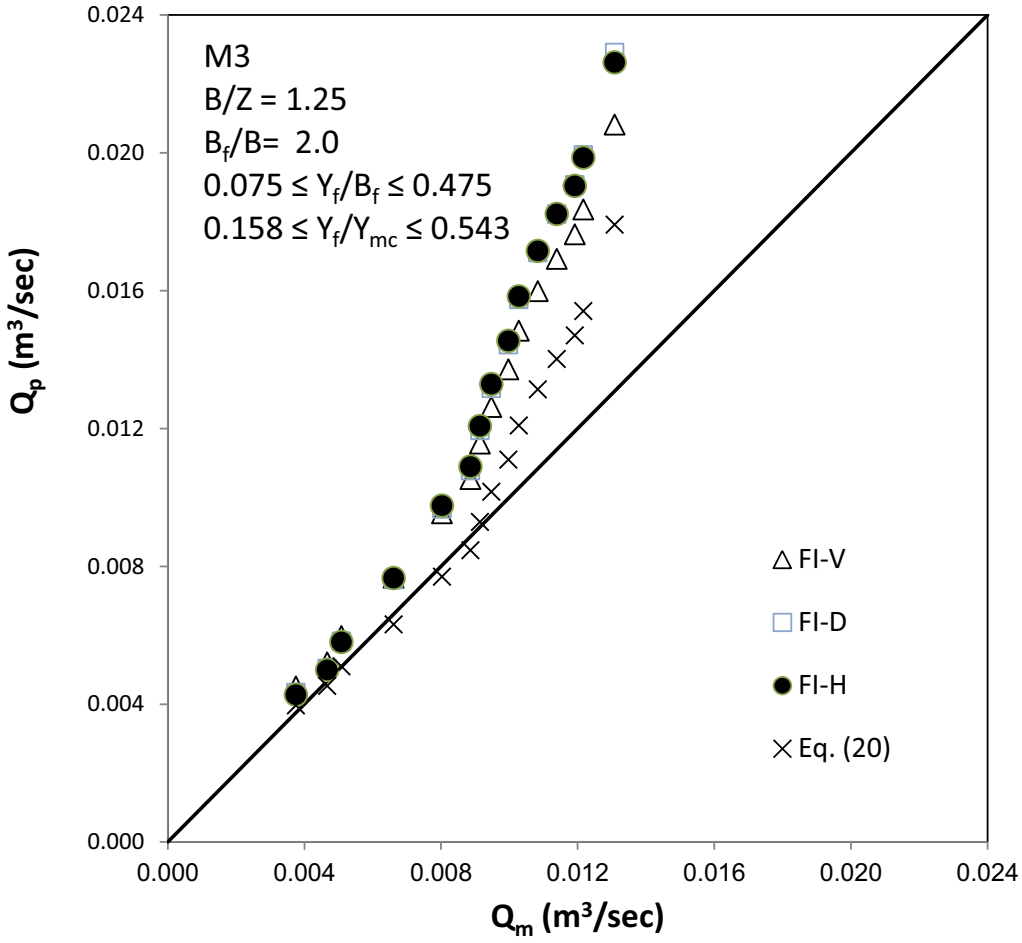

Fig. 7. Comparison of discharge calculation methods by introducing the value of τ_a from Eq. (17) with measured discharges for model M3

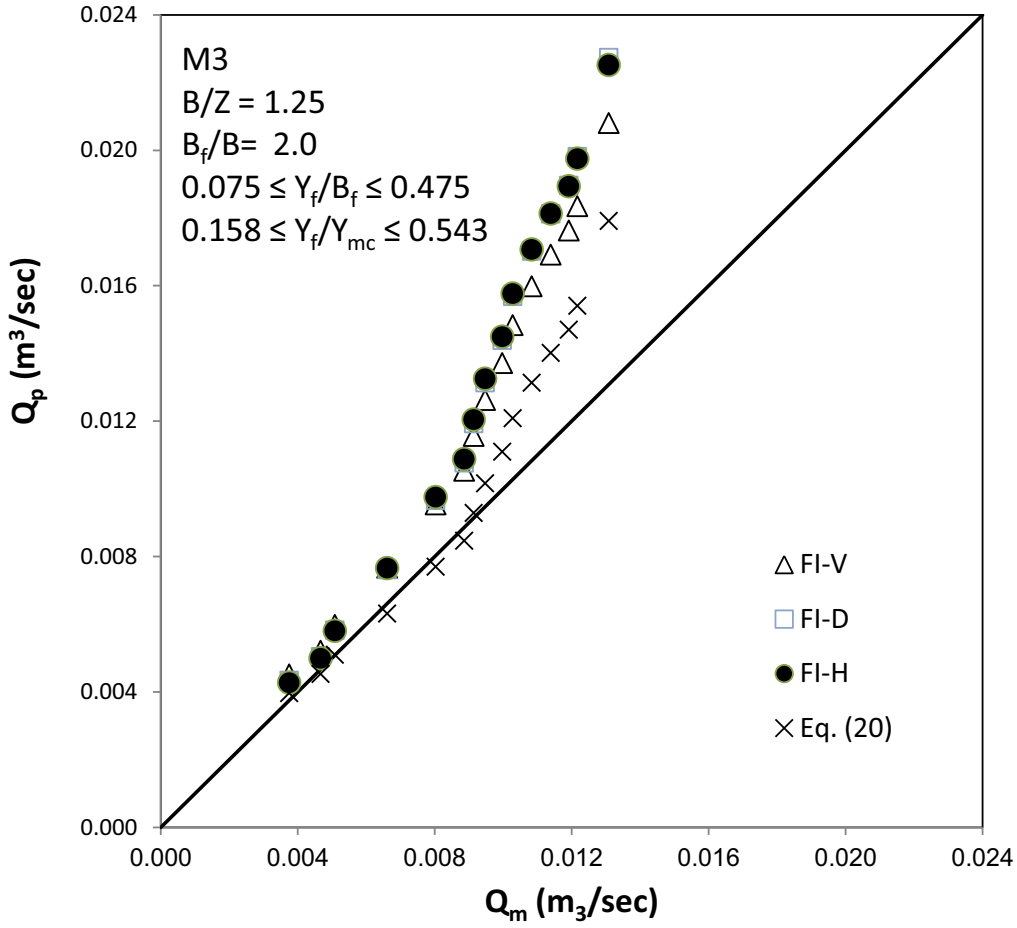

Fig. 8. Comparison of discharge calculation methods by introducing the value of τ_a from Eq. (18) with measured discharges for model M3

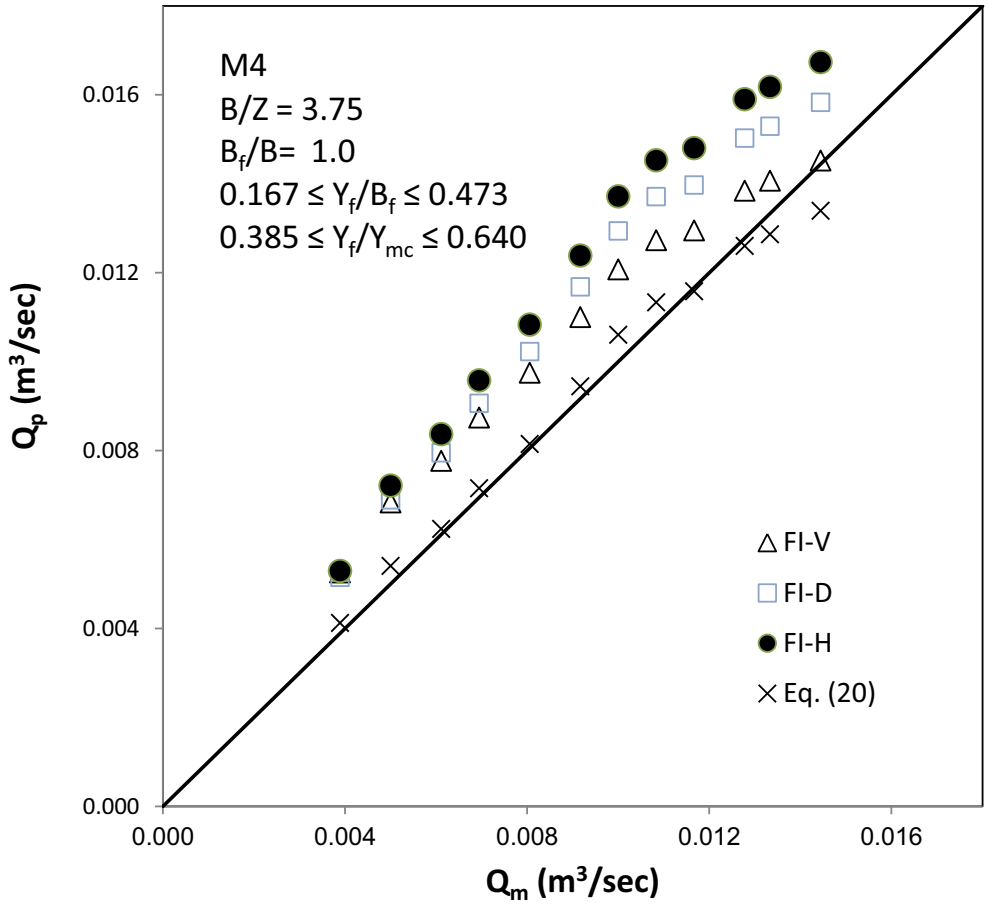

Fig. 9. Comparison of discharge calculation methods by introducing the value of τ_a from Eq. (16) with measured discharges for model M4

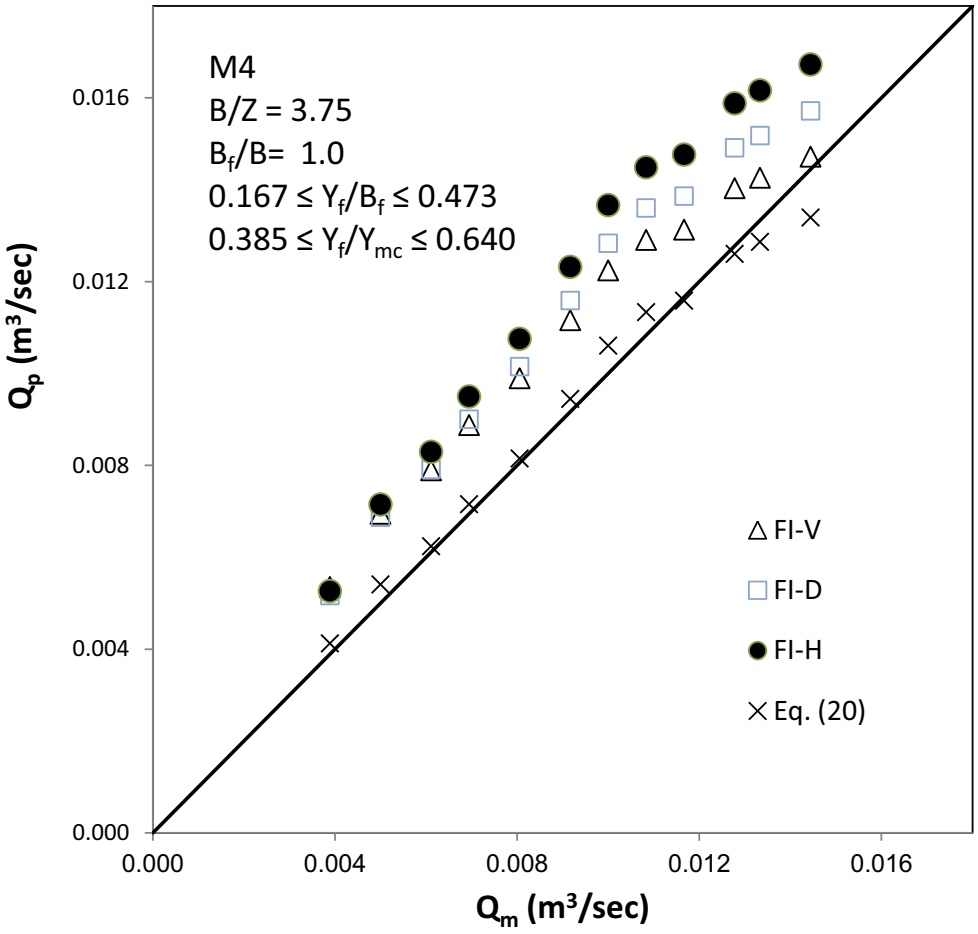

Fig. 10. Comparison of discharge calculation methods by introducing the value of τ_a from Eq. (17) with measured discharges for model M4

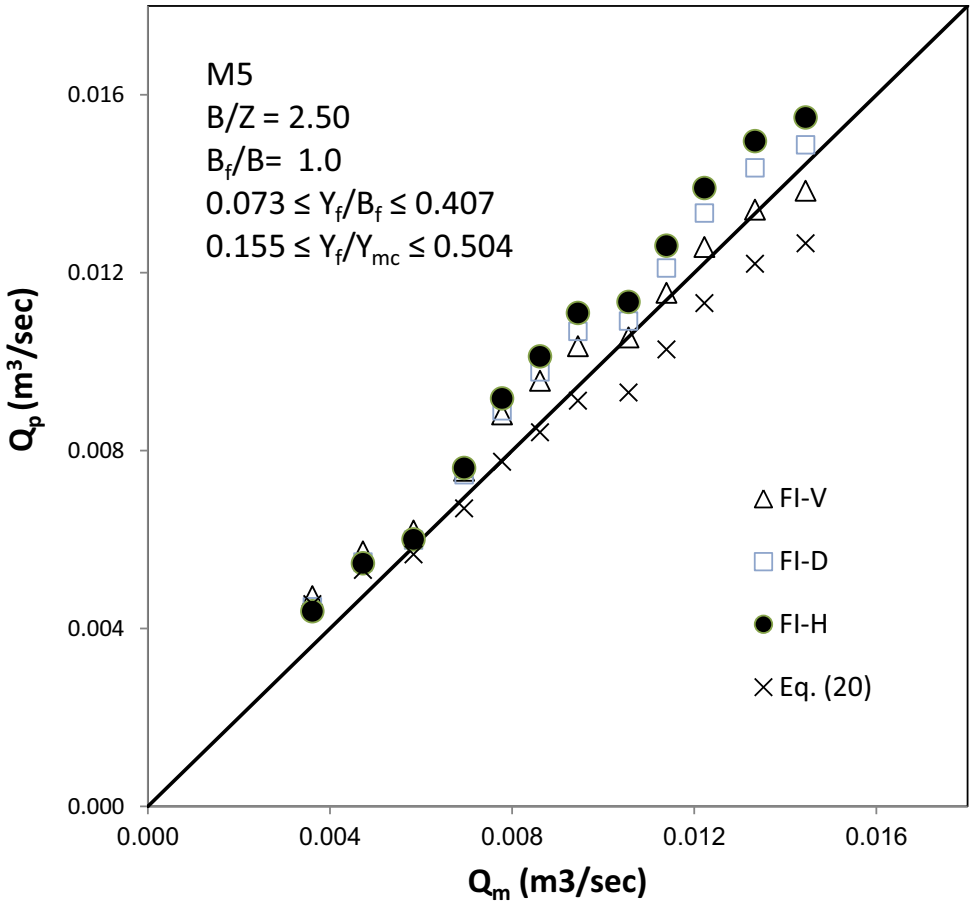

Fig. 11. Comparison of discharge calculation methods by introducing the value of τ_a from Eq. (16) with measured discharges for model M5

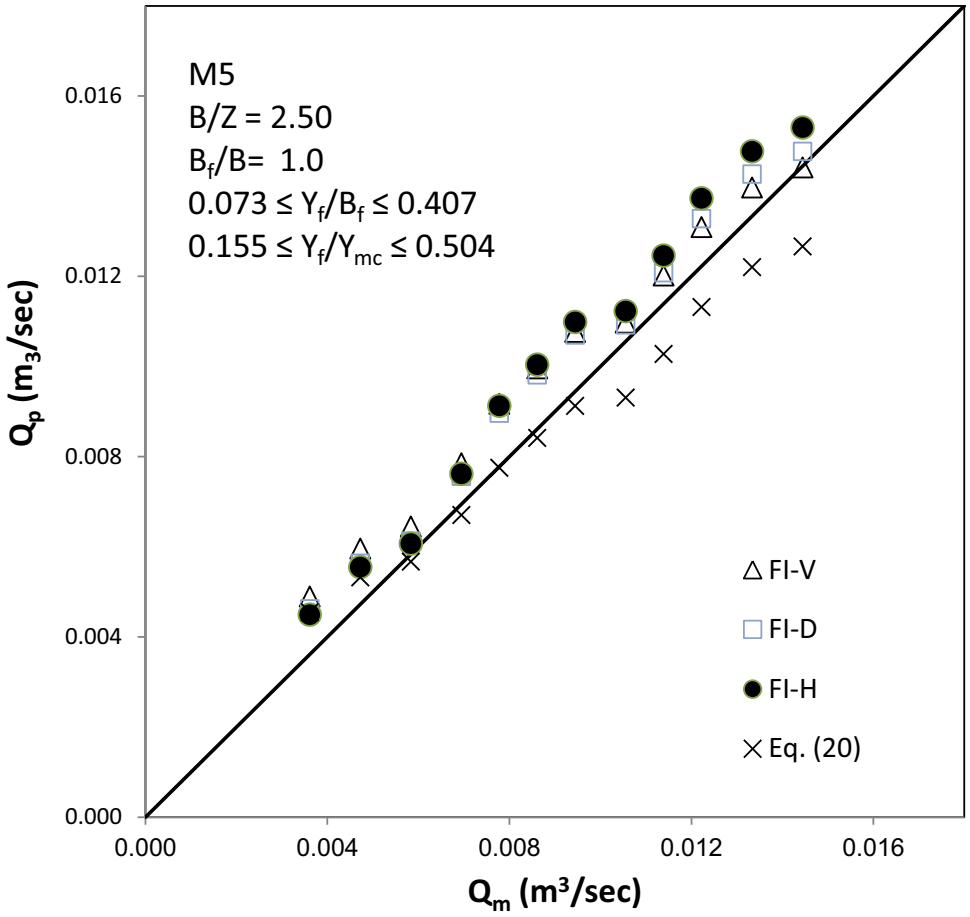

Fig. 12. Comparison of discharge calculation methods by introducing the value of τ_a from Eq. (18) with measured discharges for model M5

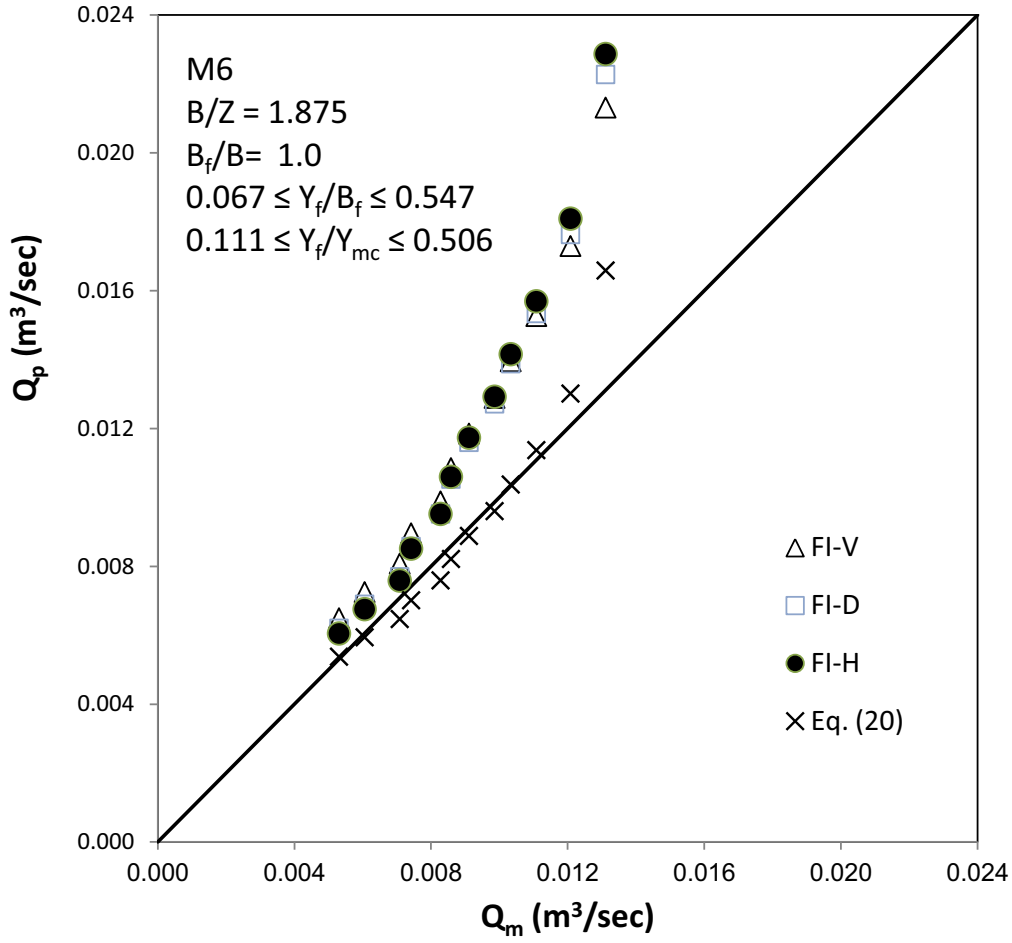

Fig. 13. Comparison of discharge calculation methods by introducing the value of τ_a from Eq. (17) with measured discharges for model M6

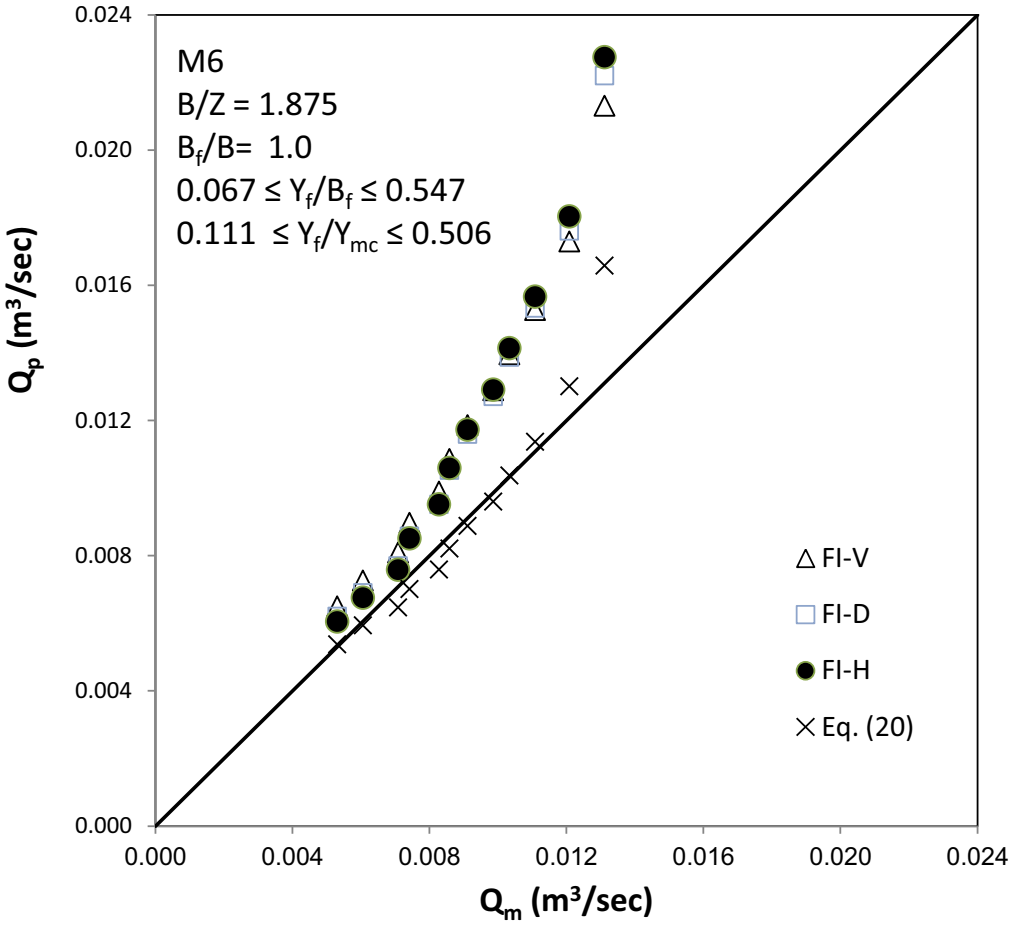

Fig. 14. Comparison of discharge calculation methods by introducing the value of τ_a from Eq. (18) with measured discharges for model M6

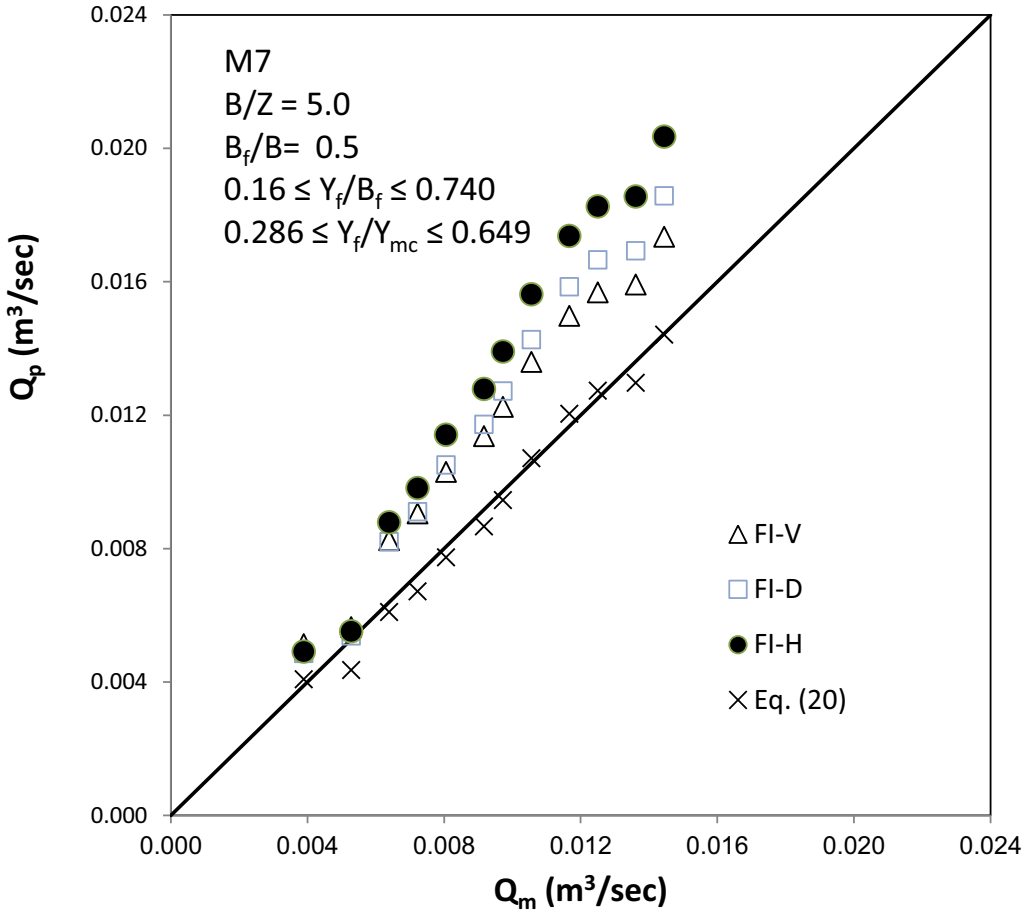

Fig. 15. Comparison of discharge calculation methods by introducing the value of τ_a from Eq. (16) with measured discharges for model M7

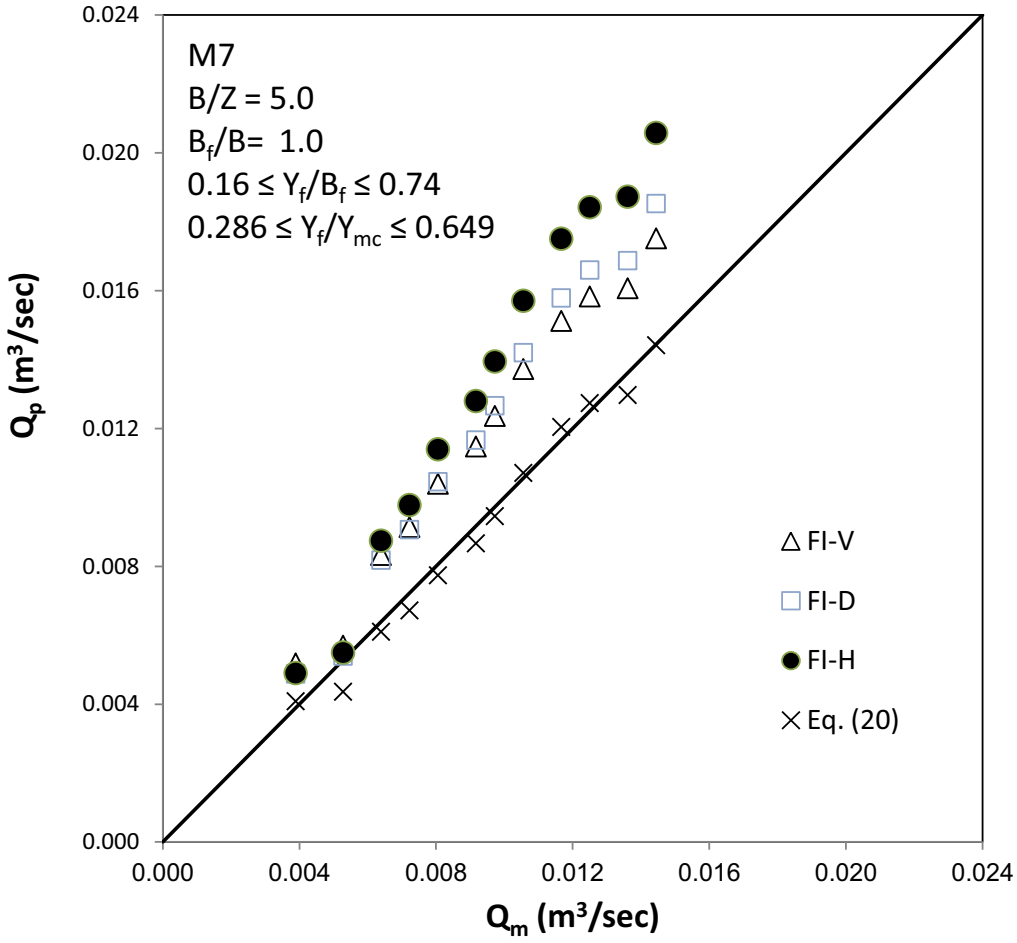

Fig. 16. Comparison of discharge calculation methods by introducing the value of τ_a from Eq. (17) with measured discharges for model M7

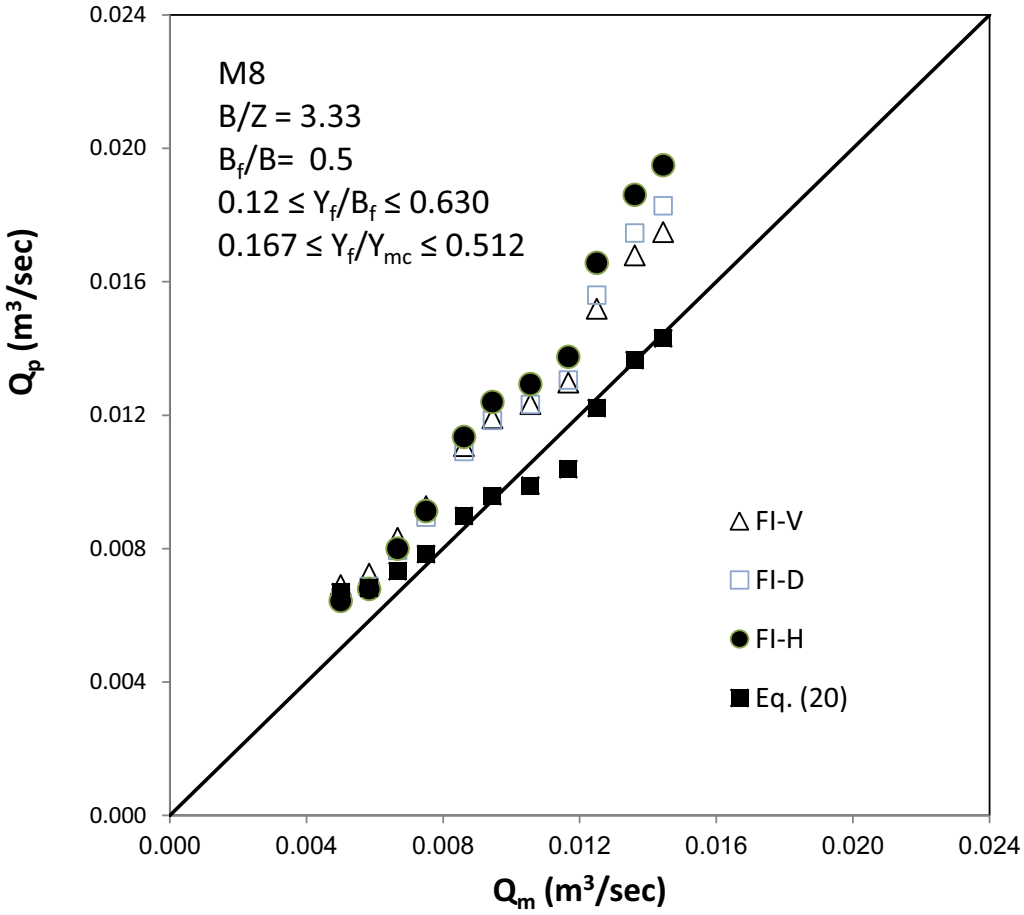

Fig. 17. Comparison of discharge calculation methods by introducing the value of τ_a from Eq. (16) with measured discharges for model M8

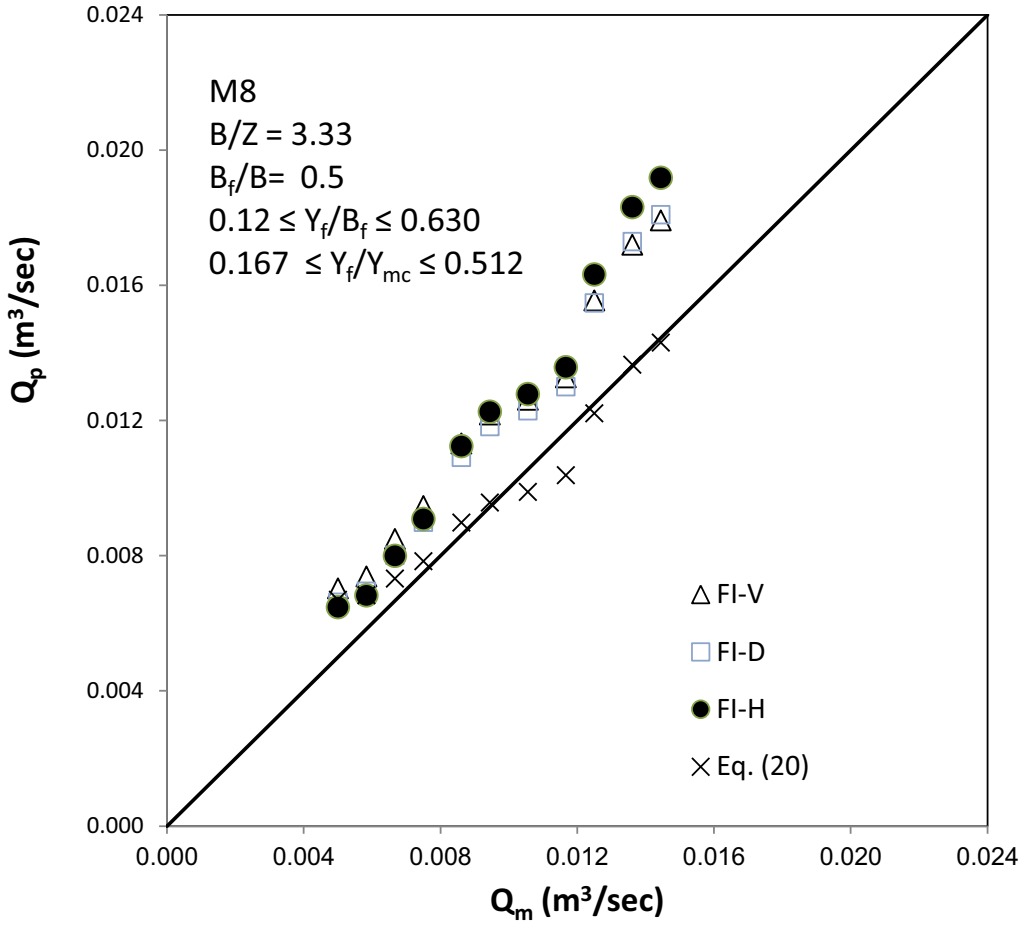

Fig. 18. Comparison of discharge calculation methods by introducing the value of τ_a from Eq. (18) with measured discharges for model M8

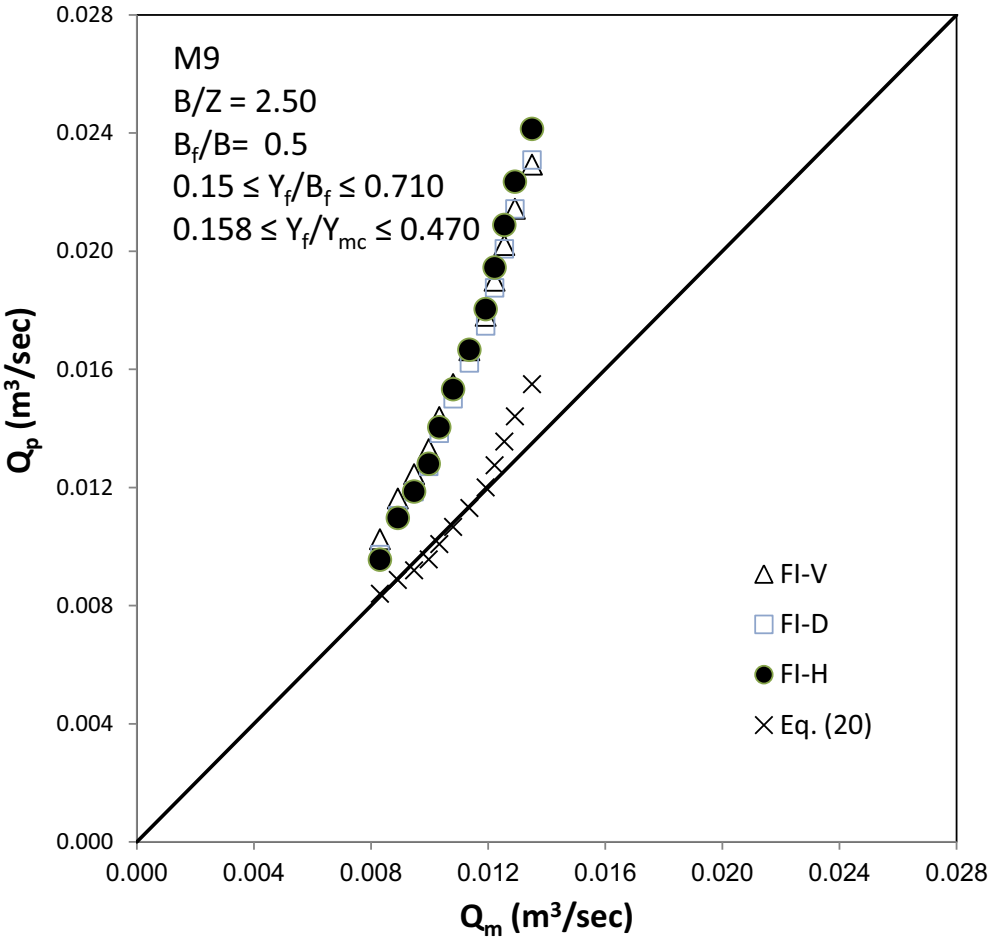

Fig. 19. Comparison of discharge calculation methods by introducing the value of τ_a from Eq. (17) with measured discharges for model M9

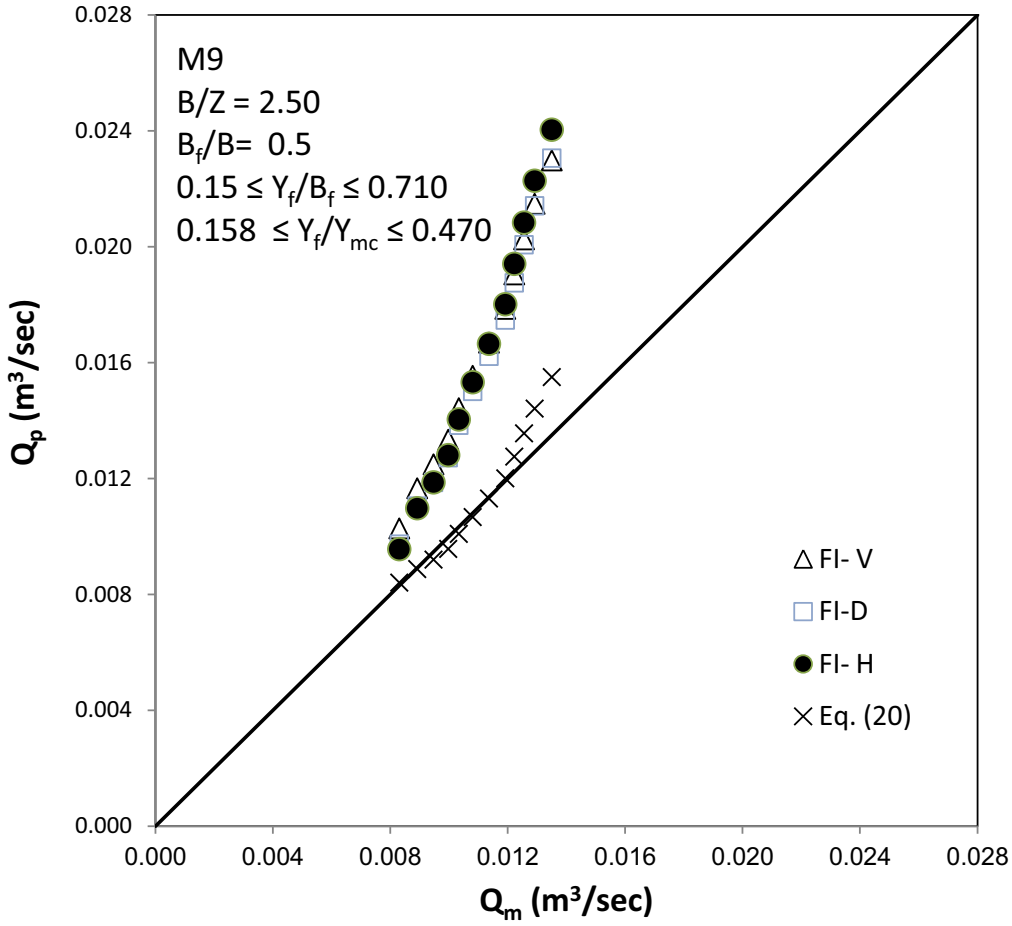

Fig. 20. Comparison of discharge calculation methods by introducing the value of τ_a from Eq. (18) with measured discharges for model M9